Direct metal micropatterning on needle-type structures towards bioimpedance and chemical sensing applications

2015 J. Micromech. Microeng. 25 015002

(http://iopscience.iop.org/0960-1317/25/1/015002)

IOP Publishing Journal of Micromechanics and Microengineering
J. Micromech. Microeng. **25** (2015) 015002 (10pp) doi:10.1088/0960-1317/25/1/015002

Direct metal micropatterning on needle-type structures towards bioimpedance and chemical sensing applications

Sanghyeok Kim[1,4], Jae-ho Park[1,4], Kyungnam Kang[1,2], Chong-Ook Park[2,3] and Inkyu Park[1,2]

[1] Department of Mechanical Engineering, Korea Advanced Institute of Science and Technology (KAIST), Daejeon, 305–701, Korea
[2] KI for the NanoCentury & Mobile Sensor and IT Convergence (MOSAIC) center, KAIST, Daejeon, 305–701, Korea
[3] Department of Materials Science and Engineering, KAIST, Daejeon, 305–701, Korea

E-mail: inkyu@kaist.ac.kr

Received 4 September 2014, revised 15 October 2014
Accepted for publication 17 October 2014
Published 5 December 2014

Abstract

Direct metal patterning methods, such as screen printing, inkjet printing and gravure/flexography printing, are widely used to form electrodes or interconnections for printed electronic devices due to their inexpensive, simple and rapid fabrication as compared to vacuum-based conventional metallization processes. Here, we present direct metal patterning by modified screen printing on the curved surface of needle-type rod structures (i.e. rods with radius of $\rho < 1$ mm). We achieved various microscale patterns such as straight lines, zigzag lines, wavy lines and alphabetic words with a minimum width of 70 μm on the surface of the rod. Also, four pairs of line patterns were printed on the single rod for electrical interconnection. Printed patterns on the surface of the rod were used as electrodes for the control of a light emission diode (LED) as well as the real-time electrochemical impedance spectroscopy of electrolyte solutions and solid objects by the rod insertion. Furthermore, needles with multiple pairs of microelectrodes were used to measure the electrical impedance of biological samples such as fat and muscle tissues of porcine meat. In addition, a needle-type probe sensor with gas sensing capability was demonstrated by using a needle with printed Ag electrodes and Pd thin films.

Keywords: screen printing, metal patterning, impedance spectroscopy, electrochemical sensor, gas sensor, bioassay, curved substrate

S Online supplementary data available from stacks.iop.org/JMM/25/015002

(Some figures may appear in colour only in the online journal)

1. Introduction

Recently, novel electronic devices such as sensors [1–6], display devices [7–9] and batteries [10, 11] fabricated on small curved or flexible substrates have attracted significant attention as human-friendly and wearable devices. They can be used as wearable electronic devices [2–4] or motion detection devices [3, 4] attached on human body as well as biocompatible objects for the measurement of the electrochemical properties of biological tissues [5, 6]. However, conventional microfabrication approaches based on photolithography and vacuum-based thin film deposition processes are not suitable for patterning metal electrodes and interconnections on

[4] Author to whom any correspondence should be addressed.
These authors equally contributed to this work.

small curved surfaces. Alternative methods such as modified optical lithography using flexible photomasks [12] or flexible dry photoresists [13], micro-contact printing [14], pad printing [7], *in situ* microfluidic method [15], laser structuring [16] and the 3D conformal printing technique [17] have been developed for microscale patterning on curved surfaces. By using these methods, patterning of functional materials of various shapes can be achieved on non-flat surfaces and used for electronic devices such as displays [7], temperature detection sensors [13] and small antennas [17] on curved structures. However, these processes have been demonstrated only on curved surfaces with relatively large radii of curvature (a few mm–a few cm [7, 12, 13, 15–17]) and require multistep fabrication processes including photoresist transfer and developing steps [12, 13] or involve a wet chemical etching procedure [14]. Although the fabrication of three-dimensionally curved micro-structures by 3D additive printing has been developed [17, 18], to the best of our knowledge, few studies have demonstrated direct micro-patterning on small curvilinear substrates (curvature radius < 1 mm).

In this paper, we present a simple direct metal patterning method for the curved surfaces of rods with very small radius (ρ < 1 mm) by using modified screen printing. We fabricate various microscale patterns, such as arrays of straight lines, zigzag lines and alphabetic words with a minimum feature size of 70 μm. Also, four pairs of line patterns are printed on the single rod for electrical interconnection of electronic devices. As applications, printed patterns on the surface of the rod are used as electrodes for the control of a light emission diode (LED) and the electrochemical impedance spectroscopy of liquid and solid objects. In addition, we demonstrate integration of the needles with an impedance sensor for biological tissue analysis and needle-type probe with gas sensing capability.

2. Experimental

2.1. Metal patterning process on the rod

Conventional screen printing systems are typically designed for large and flat substrates. Therefore, special jigs have to be designed for screen printing on the small curved surfaces of rod structures. A jig equipped with vacuum-connected v-grooves was custom-designed, as shown in figure 1. The v-grooves with depths of 1, 1.5 and 2 mm were designed to fix the rods with radii (ρ) of 0.5, 0.75, and 1 mm, respectively, in order to achieve a conformal contact between the top surface of the rod and the screen mesh without severe deformation of the mesh patterns for accurate pattern transfer to the rod surface. 15 cm-long stainless steel (SUS 304) rods with radii of 0.5–1 mm (RF medical, Korea) were used as the target substrate. The surface of each rod was covered with polyethylene terephthalate (PET) by using the thermal contraction method for electrical insulation and creating a smooth surface. Figure panels 1(*a*) and (*b*) show the photographic images and schematics of the fabrication processes of the modified screen printing system with vacuum-connected grooved jigs. As the first step of screen printing, the rod was fixed on the grooved jig. Then, conductive silver (Ag) paste ink (TEC-PA-051, Inktec, Korea) was spread onto the screen mesh. The metal content and viscosity of the Ag paste were 70 wt% and 185 000 cP, respectively. After several contacts between the squeegee and Ag paste, the squeegee was pressed down along the axial direction of the rod. Finally, the rod with printed Ag patterns was sintered in a convection oven at 120 °C for 20 min in order to remove solvent and to solidify Ag structures. Also, figure 1(*c*) shows the fabrication flowchart for multiple patterning on the rod. After the patterning and annealing processes for the first pattern, the rod is rotated by certain angle (e.g. 90°) and then a second pattern is screen printed on the top surface of the rod. By repeating these patterning cycles, we can achieve multiple patterns on a single rod. For comparison, conventional screen printing was also carried out on a flat, 75 μm thick PET substrate. The fabricated Ag structures on the rods were observed by using an optical microscope and a scanning electron microscope (SEM).

2.2. Electrical characterization of the printed metal patterns

The electrical characteristics of the Ag patterns were measured by using the two-point probe measurement method. In order to control the LEDs, the first Ag electrode line pattern was screen printed on the top surface of the rod. After the sintering process, the second line was screen printed on the opposite side. Then, the LEDs were connected with the Ag electrode lines on the rod. Electrical power for the control of the LEDs was supplied to the Ag electrode line patterns by using a dc power supply.

2.3. Impedance sensor for NaCl solution and conductive rubber

NaCl (7548-4400, Daejung Chemicals & Metals, Korea) solution was used as the target solution for the electrochemical impedance spectroscopy test. NaCl was dissolved in DI water with various concentrations (0.01 M, 0.05 M, and 0.1 M). In order to make a solid sample for electrochemical impedance testing, polydimethylsiloxane (PDMS) (Sylgard 184, Dow Corning, USA) was poured on the carbon black-silicone compound based conductive rubber (HR-1526, HRS, Korea) and then cured in a convection oven at 75 °C for 2 h. For impedance measurement, one end of the rod was inserted into the target solution or PDMS body with conductive silicone rubber, while other end was connected to the impedance analyzer (HP4192A, Hewlett Packard, USA).

2.4. Impedance sensor for biological tissue

Porcine meat slaughtered one day before the experiment was used for the demonstration of biological tissue measurement. In order to achieve the multi-point impedance measurement, a switch unit (34970A, Agilent Technologies, USA) and a switch module (34904A, Agilent Technologies, USA) were connected between the impedance analyzer and electrode pairs on the needle. In order to measure the difference

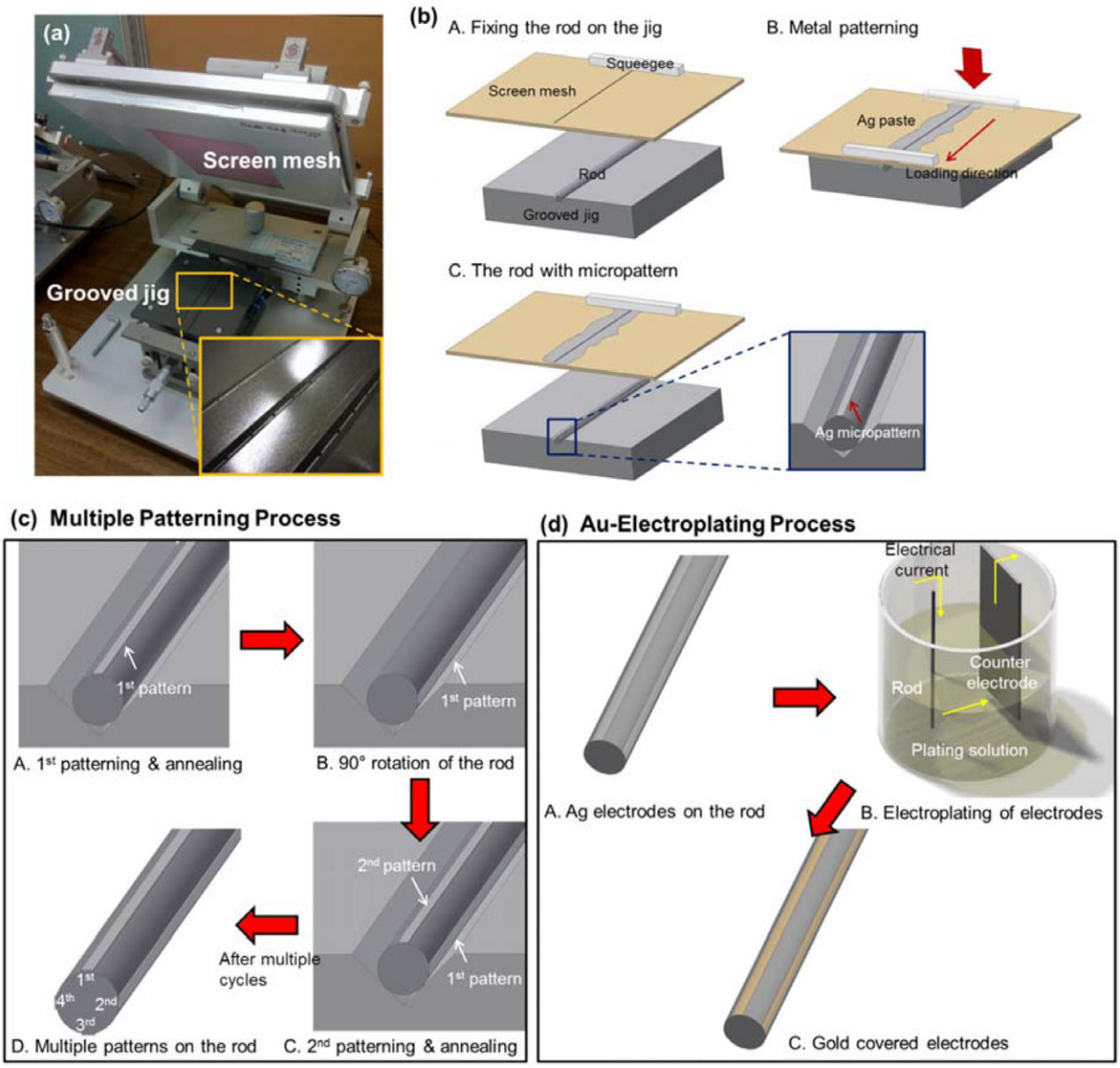

Figure 1. Fabrication setup and process flow: (*a*) modified screen printing system with vacuum-connected grooved jigs (inset); (*b*) schematic of metal patterning process on the rod: A. fixing the rod on the grooved jig, B. Ag patterning on the top surface of the rod, C. fabricated Ag micropattern on the rod; (*c*) schematic of multiple patterning process on the rod; (*d*) schematic of electroplating process of Au on the Ag pattern.

between the electrical impedances at different depths of the tissue, two pairs of Ag line electrodes with length difference of 1 cm from the needle tip were printed on the needle rod. Figure 1(*d*) illustrates the Au-electroplating process on Ag electrodes. Since gold (Au) is biocompatible, the surface of the Ag electrodes on the needle was electroplated with a 1 μm-thick Au layer by dipping the needle into the Au electroplating solution (CNC Tech., Korea) and supplying a current density of 1 mA cm^{-2} to the electrodes for 1,000 s.

2.5. Probe-type gas sensor for H_2 detection

The H_2 detection test was conducted by using a probe-type gas sensor based on Ag electrodes and palladium (Pd) thin films fabricated on the rod. After patterning and sintering a pair of the Ag line electrodes on the rod, Pd thin film with a thickness of 30 nm was deposited on the tip of the needle rod (20 × 1.5 mm^2) by using electron beam evaporation. 1% H_2 gas and air were alternately injected into the gas chamber at room temperature (25 °C). Flow rate and concentration of the gas were controlled by a mass flow controller. A voltage of 0.1 V was supplied by using a source meter (2636B, Keithley, USA) in order to measure the change of the resistance of the Pd thin film on the rod.

3. Results and discussion

If the screen mesh and rod have no initial gap without external pressure applied, printed Ag patterns are spread excessively and distorted when external pressure is given. However, when

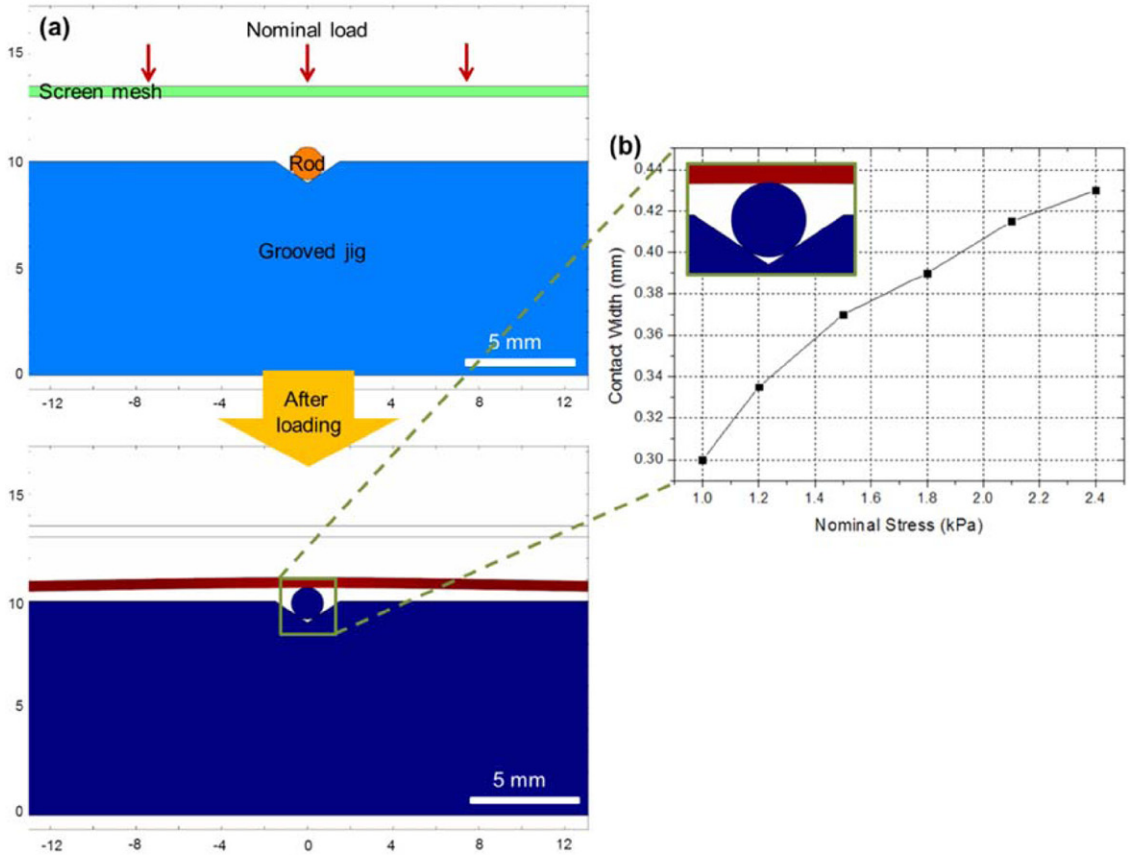

Figure 2. Numerical simulation of mesh-rod contact: (*a*) numerical simulation result of deformation of screen mesh by nominal stress before and after loading; (*b*) numerical simulation of contact width between the screen mesh and the rod at different nominal pressure. After loading, the screen mesh formed a conformal contact with the top surface of the rod with maximum contact width of 430 μm by nominal pressure of 24 kPa.

the initial gap between the screen mesh and rod is larger than 1 cm without external pressure applied, almost no contact between mesh and rod occurs even if very large pressure is applied. By experimental analysis, we achieved an optimized initial gap of 3 mm between the screen mesh and rod for accurate and clean patterning on the top surface of the rod. To confirm the validity of experimental results, we carried out a numerical simulation of the deformation of the screen mesh and its contact with the rod by using COMSOL Multiphysics® software (see figure 2). The initial gap between the screen mesh and the rod was set as 3 mm. Due to its mechanical flexibility, the screen mesh formed a conformal contact only with the top surface of the rod under uniform vertical pressure. Figure 2(*b*) shows the width of contact between the screen mesh and the rod under various nominal pressures applied on the mesh. The contact width was gradually increased from 300 to 430 μm by nominal pressures from 10 to 24 kPa.

Figure 3 panels (*a–d*) show the photographic and optical microscope images of the micropatterning results on rods and on flat PET substrate. Here, it should be noted that the stainless steel rod was also coated with a PET tube (thickness = ~80 μm) by using the thermal contraction method for electrical insulation and to form a smooth surface. Straight-line patterns with widths of 70 μm and 100 μm were fabricated without blurring of the Ag paste on the rods with ρ = 0.5 mm (figure 3(*b*)) and 1 mm (figure 3(*c*)), respectively, In addition, straight line patterns with widths of 100 μm were fabricated on the PET substrate for comparison with those on the rod (figure 3(*d*)). Although the surface of the rod is curved without a flat area, there were no significant differences in the shape and size between the rod and the flat PET substrate. In addition to the straight line patterns, we successfully fabricated various Ag micropatterns such as zigzag lines, square lines, and alphabetic words on the rods. Figure 3 panels (*e–g*) show the optical microscope and SEM images of various Ag structures on the rods with radius of ρ = 0.75 mm. From the SEM images, we observed that the Ag structures were clearly defined with Ag micro/nanoparticles without significant pattern distortion. The printed patterns were composed of randomly shaped Ag particles with sizes of 100 nm–500 nm, whose surfaces were covered with smaller Ag nanoparticles with sizes of 10 nm–40 nm (See the Supporting Information, figure S1 (stacks.iop.org/JMM/25/015002)). However, slight spreading of Ag particles occurred at the pattern edges due to the wetting of Ag paste during the printing process. Furthermore, multiple parallel Ag line array patterns were fabricated on the rod (ρ = 0.75 mm), as shown in figures 3(*h*)–(*j*). Figure 3(*i*) shows the optical microscope and SEM images of the first and second parallel line arrays on the rod. Through this repeated printing process, four pairs of parallel Ag line array patterns with uniform interval could be fabricated along the surface of the rod, which provides several electrical

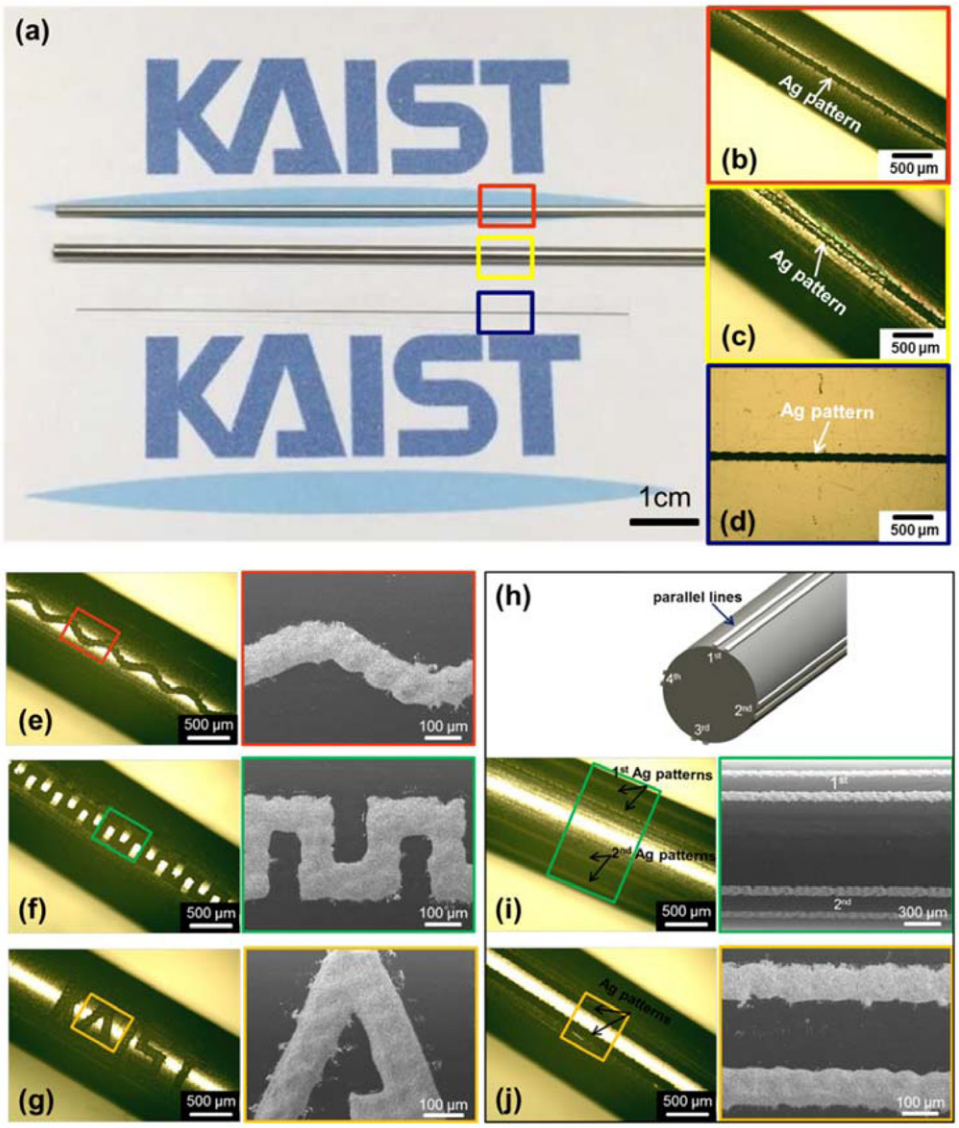

Figure 3. Results of metal patterning on rods: (*a*) photograph image of micropatterning results on the rods with radii (ρ) of 0.5 and 1 mm and on the flat PET substrate; (*b* and *c*) straight line patterns (width (W) = 70 μm and 100 μm) on the rods (ρ = 0.5 mm and 1 mm); (*d*) straight line pattern (W = 100 μm) on the PET substrate; Optical microscope and SEM images of various micropatterns on the rod (radius ρ = 0.75 mm); (*e*) zigzag line; (*f*) square line; (*g*) alphabetical words; (*h*) schematic diagram of the rod with four pairs of electrodes; (*i*) first and second parallel lines in four pairs of electrodes; and (*j*) single pair of parallel lines on the rod.

interconnection paths on a single rod. Higher resolution optical microscope and SEM images of the single parallel line pair are shown in figure 3(*j*). Wavy shapes were observed at the pattern edges due to the wetting of Ag paste along the screen mesh during the screen printing process. However, the average widths of the printed parallel line patterns were uniform, and were the same as those of the designed patterns in the screen mesh. We observed the surface by using an optical microscope and measured the electrical resistivity of the line pattern on the rod after each sintering step in order to confirm the effect of sintering time on the surface morphology and electrical conductivity of line pattern (see the Supporting Information, figure S2 (stacks.iop.org/JMM/25/015002)). From the experimental results, we verified that there were no significant changes in the electrical resistivity, line width and pattern morphologies after several sintering steps (maximum sintering number = 4; 20 min each). As shown in these patterning results, we can confirm that the fine patterning of multiple microstructures on small-diameter rod is possible by using the modified screen printing process.

Metal micropatterns made by direct metal printing on rods can be used as electrodes or interconnections for electronic devices. Figure 4(*a*) shows the statistics of electrical resistivity of Ag line patterns on the rod. All Ag patterns on the rod showed ohmic resistor behavior with an average resistivity of $7.17 \times 10^{-7}\,\Omega$·m (standard deviation=$1.47 \times 10^{-7}\,\Omega$·m), which is 45 times higher than that of bulk Ag ($1.6 \times 10^{-8}\,\Omega$·m). The higher resistivity of conductive Ag paste could be due to the porous morphology of Ag structures (see the Supporting Information, figure S1 (stacks.iop.org/JMM/25/015002)) and remaining organic materials after the thermal sintering process [19–21].

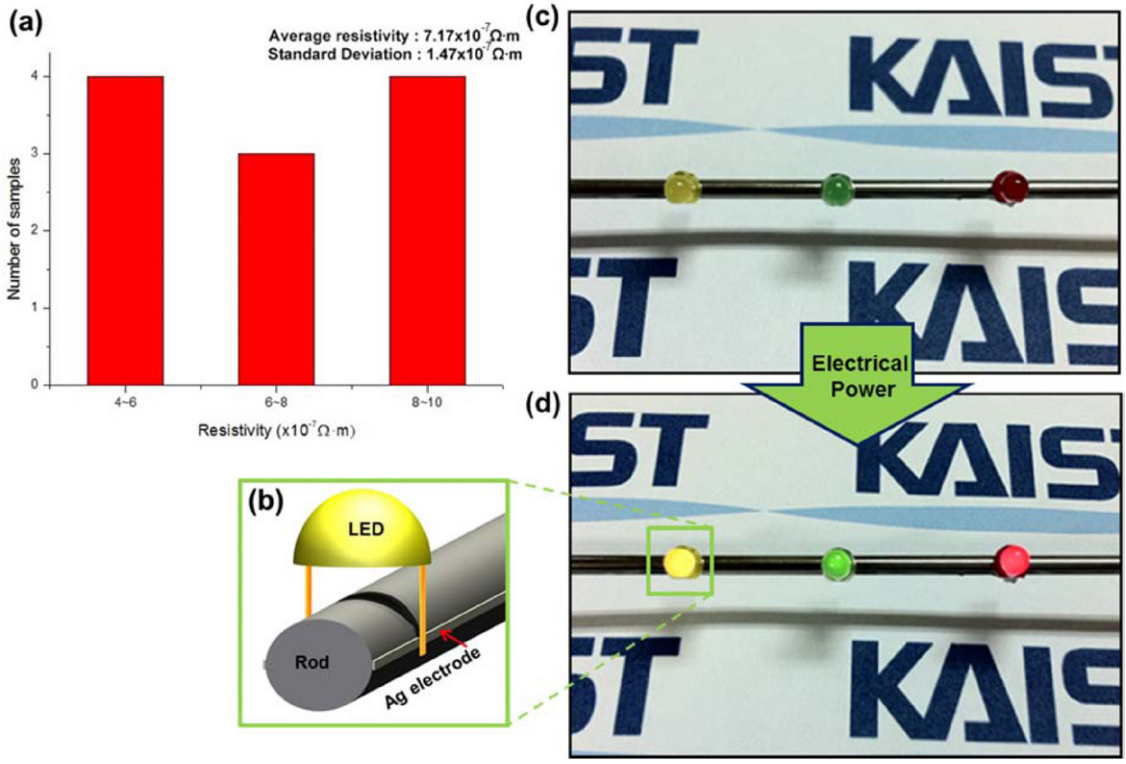

Figure 4. Electrical characteristics of printed metal patterns: (*a*) statistics of calculated electrical resistivity of various electrode patterns on the rods with average resistivity of 7.17 × $10^{-7}\,\Omega$·m and standard deviation of 1.47 × $10^{-7}\,\Omega$·m; (*b*) schematic diagram of an LED connected by Ag electrode patterns; (*c* and *d*) LEDs connected by Ag electrode patterns on the rods before (*c*) and after (*d*) supplying the electrical power.

As an application, we used printed Ag patterns on the rod as the metal electrodes for the control of LEDs. Figure 4 panels (*c* and *d*) show photographic images of the rod with LEDs before and after supplying the electrical power. The LEDs were turned on by supplying an electrical voltage of 2 V across two Ag electrodes. From this result, we verified that the Ag line patterns on the rod could be successfully used as electrodes for tiny electronic devices operating on small curved structures such as small-diameter rods. As more practical application, Ag line patterns on the rod were used as electrodes for probe-type electrochemical impedance measurement device. Figures 5(*a*) and (*b*) show the experimental setup for impedance measurement and analysis results for NaCl solutions with various concentrations (0.01 M, 0.05 M, and 0.1 M). The higher the concentration of NaCl solution is, the higher the conductance becomes in all frequencies from 1 kHz to 1 MHz. This kind of device can be potentially used as the electrochemical analysis probe to monitor local chemical information in liquid environment. This needle-type probe device can also be used for the impedance analysis of solid-phase samples. As an example, the device was used for the real-time impedance measurement of conductive silicone rubber embedded in non-conductive PDMS body (see figure 5(*c*)). Figure 5(*d*) shows the conductance data measured during the insertion of the needle into the PDMS. Before the needle tip entered the conductive rubber region, the average conductance was measured at 3.05 × 10^{-7} S. However, when the needle tip was inserted into the conductive silicon rubber, the measured conductance was instantly increased by four orders of magnitude (3.25 × 10^{-3} S). After the needle was pulled out from the conductive silicone rubber, the impedance recovered to the initial value. From this experimental result, we demonstrate that the real-time impedance measurement of solid materials could be accomplished by the insertion of the needle integrated with impedance measurement electrodes.

The needle integrated with impedance sensor array could be used in biomedical applications. Rods with very small diameters (D < 1.27 mm, 18 gauge) are commonly used as clinical needles for biopsy or treatment of diseases. Especially, tissue biopsy by extracting suspicious lesions from the human body with a thin and hollow needle has been performed for disease diagnosis [6, 22]. Typically, ultrasound (US) and computed tomography (CT) imaging techniques have been commonly used to assess and guide the position of the needle with respect to the target tissue during the biopsy process [23, 24]. However, these methods can provide only limited resolution and accuracy of cancerous tissue detection. In the case of prostate cancer, many tissue samples have to be extracted from 6–12 locations because the lesions cannot be visualized by using US or CT techniques, thereby involving unnecessary and inaccurate extraction of prostate tissues. Although the magnetic resonance imaging (MRI) technique can provide better imaging resolution, the operation period and cost of MRI are high [22]. As an alternative method, electrical property measurement was proposed for the differentiation of normal and cancerous prostate tissues by Mishra *et al* [6, 25, 26]. Here, the electrical impedances of normal and prostate cancer tissues were measured by using the biopsy needle.

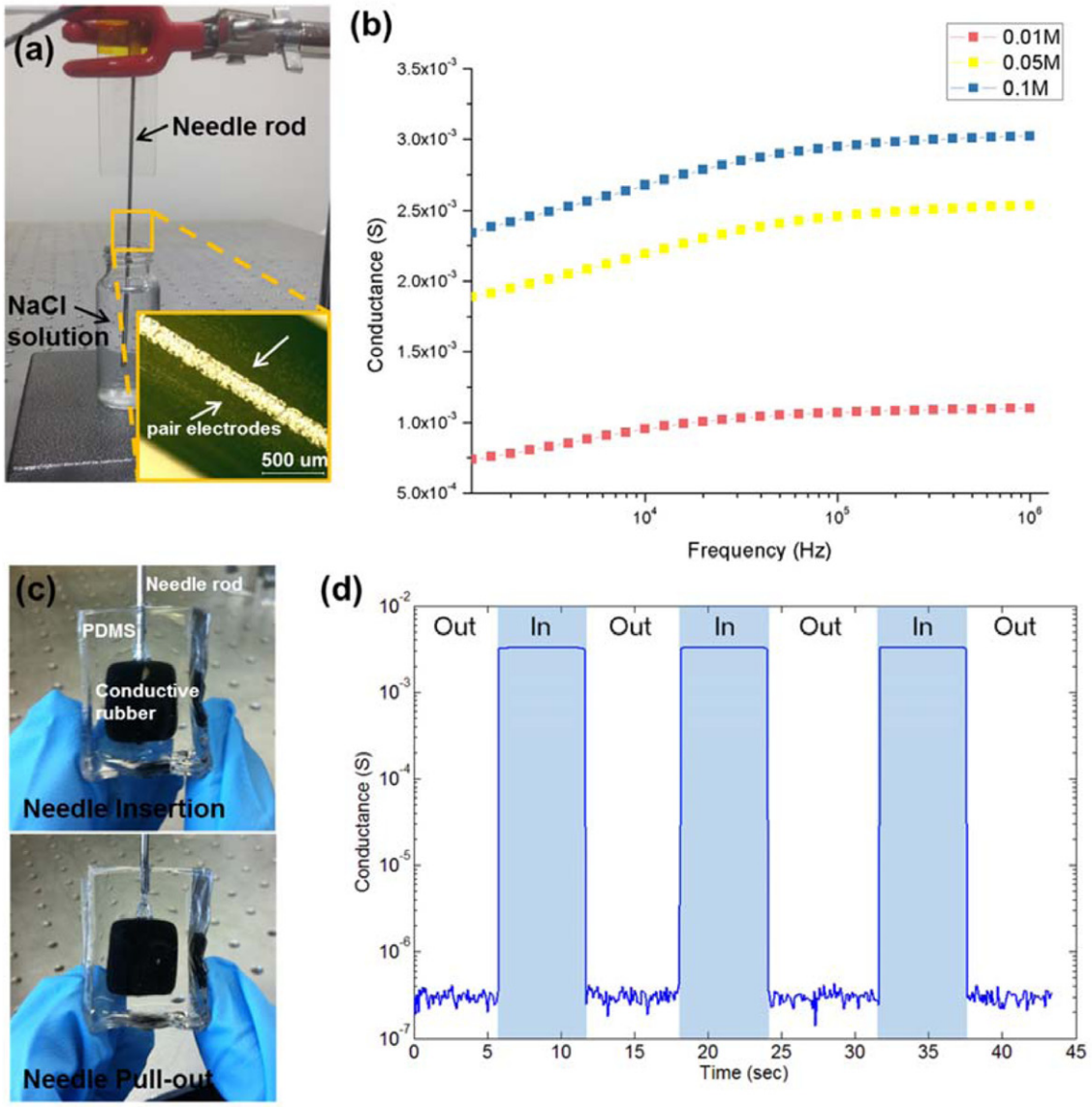

Figure 5. Applications of directly printed Ag micropatterns to liquid electrochemical and solid electrical impedance sensors: (*a*) experimental setup for impedance spectroscopy of NaCl solutions (inset: single pair of electrodes on the rod); (*b*) measured conductance of 0.01. 0.05, and 0.1 M NaCl solutions; NaCl solution with higher concentration shows higher electrical conductance; (*c*) photograph images before and after insertion of needle into the PDMS body with conductive silicone rubber; (*d*) real-time conductance measurement by repeated insertion of needle into PDMS body with conductive silicone rubber; When the sensor electrode was inserted into the conductive silicone rubber, conductance was increased by four orders of magnitude.

However, they could only measure the average electrical impedance of tissues around the needle since the whole biopsy needle was used as the electrode. Therefore, this method could not provide selective impedance measurement of local tissues near the needle tip [6]. In this work, we present the potential application of the needle with printed metal microelectrode arrays to measure the impedance of biological tissues during the biopsy process. As a proof-of-concept, we demonstrated real-time impedance measurement of different tissues in porcine meat by using a needle integrated with two pairs of impedance sensors (see figures 6(*a*) and (*b*)). In order to avoid the genotoxicity and cytotoxicity of Ag nanoparticles and to improve the biocompatibility of electrodes, their surface was coated with Au thin film by an electroplating process. After the electrodeposition, the porous surface of the Ag pattern was covered with densely packed Au thin film, which was composed of microscale grains with size of 1–5 μm. There were almost no pinholes or visible cracks at the surface of the Au thin film (see the Supporting Information, figures S3 and S4 (stacks.iop.org/JMM/25/015002)). Therefore, we could avoid the harmful effects of Ag nanoparticles on biological tissues by completely shielding the Ag patterns with biocompatible Au thin film. The sensing electrode pair E1 reached up to 2 mm from the needle tip while another pair E2 was shorter than E1 by 10 mm. This configuration allowed real-time longitudinal mapping of electrical impedance of biological samples. In order to obtain precise and reliable quantification of biological tissues independent of the sensor configurations, we converted the measured conductance (extrinsic property) into the conductivity (intrinsic property). The conductivity (σ) can

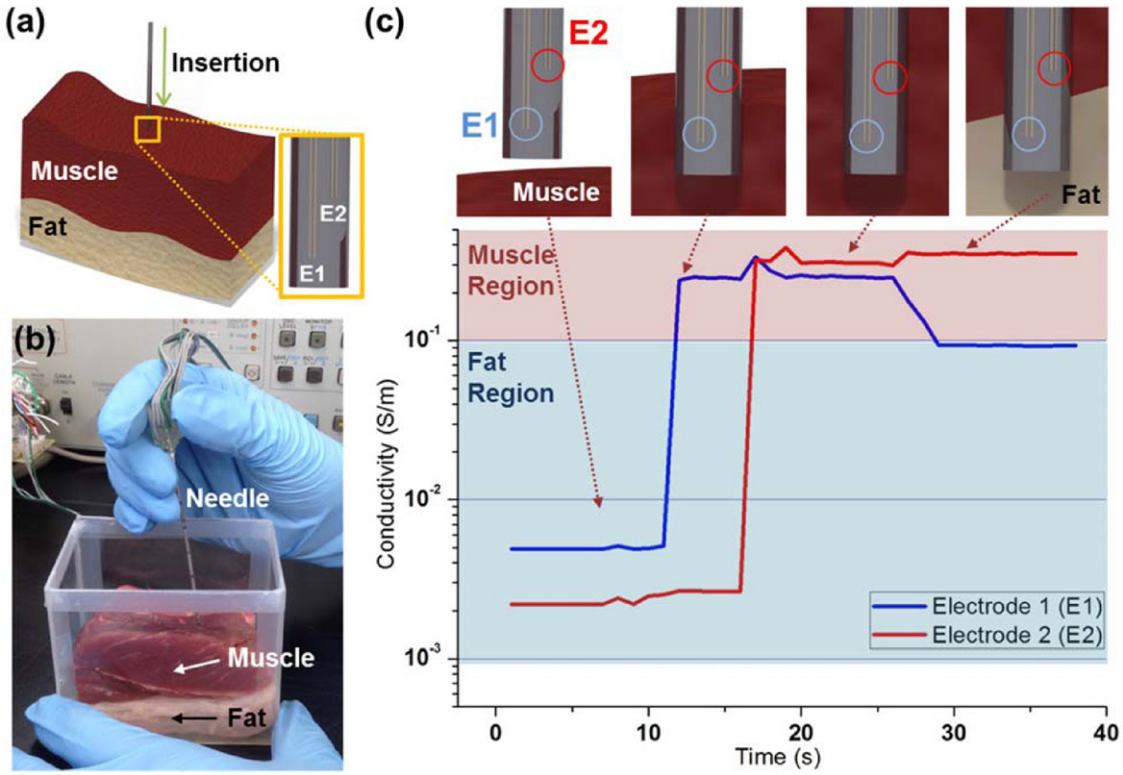

Figure 6. Electrical impedance measurement of biological tissues by using sensor integrated needle: (*a*) schematics of tissue diagnosis by sensor-integrated needle; (*b*) real photographic image of the needle insertion into the porcine meat (inset: the multi-pair electrodes on the needle); (*c*) schematics of needle insertion through the tissue and measured electrical conductivity at two sensors (E1 and E2). The electrical conductivities of both muscle and fat tissues can be measured at the same time due to the different length of electrodes of E1 and E2. The fabricated needle can be used not only for measuring the electrical conductivities of biological tissues but also for discriminating the types of tissues.

be calculated by the equation $\sigma = G/K$ where G is the measured conductance of tissue and K is the cell constant of the impedance sensor. Here, the cell constant of the impedance sensor could be calculated by using the known conductivity and measured conductance of NaCl solution. Figure 6(*c*) shows the schematics of needle insertion into the tissues and results of measured electrical conductivity of tissues at two impedance sensors. The conductivity graph shows two regions: muscle region (in light red color) with conductivity of $>0.1\,S\,m^{-1}$ and fat region (in light blue color) with conductivity between $0.001\,S\,m^{-1}$ and $0.1\,S\,m^{-1}$ [27]. When only sensor E1 got inserted into the muscle tissue, the conductivity of tissue around E1 was rapidly increased to $0.25\,S\,m^{-1}$, which is within the conductivity range of muscle tissues. However, the conductivity at E2 was maintained low ($\sim 0.02\,S\,m^{-1}$) since it was still outside the tissue. When the needle was inserted further into the tissue and the tip of sensor E2 made a contact with muscle tissue, the conductivity of tissue at E2 also increased to $0.3\,S\,m^{-1}$. Since the length of sensor E1 was longer than sensor E2 by 10 mm, we can measure the electrical conductivity of both muscle and fat tissues at the same time when the tip of the needle is located around the boundary between muscle and fat tissues. The electrical conductivity at E1 decreased to $0.09\,S\,m^{-1}$ after contact with fat tissue, while the conductivity at E2 located in the muscle tissue did not change. From this experimental result, we demonstrated that the needle integrated with impedance sensing electrodes can be used not only for measuring the impedance of biological tissues but also for controlling the penetration depth and discriminating the types of tissues during the needle insertion in the biopsy procedure.

A slender probe-type device integrated with gas sensors can be very useful for detecting bad smells inside narrow and deep holes or leakage of flammable or toxic gases within tiny cracks or cavities (e.g. a manhole or drain, as shown in figure 7(*b*)). For this purpose, we developed a probe needle integrated with gas sensor based on a pair of the screen-printed Ag electrodes and evaporated Pd thin films, as shown in figure 7(*a*). Here, the Pd thin film on the probe tip was used as a sensing material for detecting H_2 gas. When H_2 gas is exposed to the surface of Pd thin film, H_2 molecules are dissociated into hydrogen atoms ($H_2 \rightarrow 2H$). Then, the dissociated hydrogen atoms are diffused into the Pd thin film, forming a phase change of Pd to palladium hydride (PdH_x) at room temperature. Due to this phenomenon, the resistance of Pd thin film is increased by H_2 gas [1, 28, 29]. Figure 7(*c*) shows the sensor response (S) vs time for the probe-type gas sensor to 0.5% and 1.0% H_2 gas. Here, the sensor response S was defined as $S = (Rg - Ra)/Ra \times 100(\%)$ where Rg and Ra are the electrical resistances of the Pd thin film in H_2 and air environments, respectively. The gas sensing test was performed under the environment of a controlled gas chamber in real time. When H_2 gas was

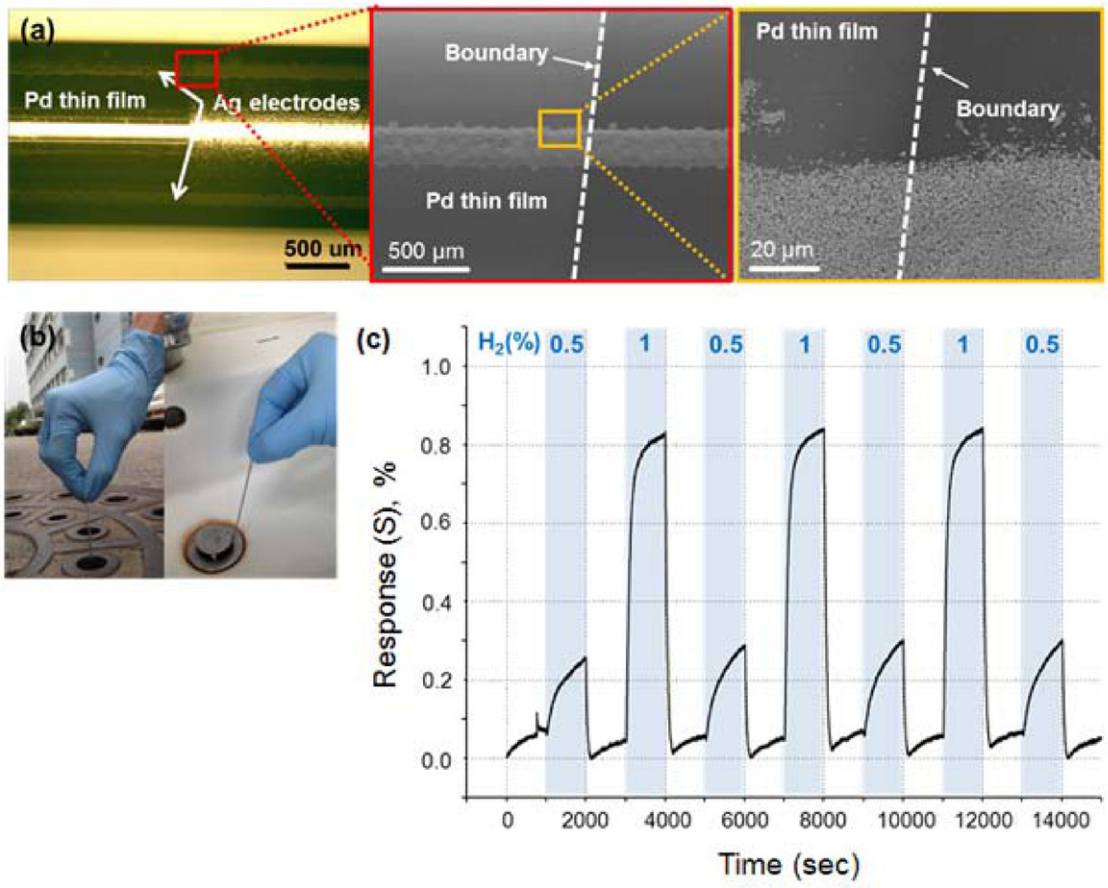

Figure 7. Probe-type gas sensor based on needle integrated with printed Ag electrodes and evaporated Pd thin film: (*a*) optical microscope and SEM images of the Pd thin film and the screen-printed Ag line electrode on the rod; (*b*) photographic images of insertion of probe-type gas sensor into narrow and deep holes such as the manhole and the drain; (*c*) real-time sensing response of the probe-type gas sensor with Pd thin film to H_2 gas (0.5 and 1%) at room temperature in a controlled gas chamber; The probe sensor showed maximum response of $S = 0.3\%$ under 0.5% of H_2 gas and $S = 0.84\%$ under 1% of H_2 gas.

injected, the sensor showed a maximum response of $S = 0.3\%$ to H_2 at 0.5% concentration. Also, at higher H_2 concentration (1%), the sensor response increased to $S = 0.84\%$. The sensor exhibited a very high signal to noise ratio (SNR) of 41.8, which indicates that the sensor can detect H_2 gas with much lower concentration. This result proves the feasibility of a probe-type gas sensor integrated with sensing films and screen printed Ag electrodes to the detection of gaseous analytes.

4. Conclusion

In conclusion, we demonstrated direct metal patterning by using a modified screen printing process on curved, small-diameter structures. Various patterns such as straight lines, zigzag lines, wavy lines and alphabetic words with minimum width of 70 μm could be successfully fabricated on the rods with radius of $\rho < 1$ mm. We have demonstrated the application of the fabricated structures to various functional devices including an LED array device on small rods, an electrochemical impedance analyzer for liquid and solid objects, a bioimpedance analyzer for diagnosis of biological tissues and probe-type gas sensors. It is believed that this direct metal micropatterning process on small curved objects can provide a very versatile, simple, high-speed, economic and reliable approach to fabricate metal electrodes or interconnections for various electronic devices such as electrochemical sensors, curved electronic devices and smart medical diagnosis tools.

Acknowledgment

This research was supported by the Center for Integrated Smart Sensors funded by the Ministry of Science, ICT and Future Planning (MSIP, Korea), Science and Technology as Global Frontier Project (CISS-2012M3A6A6054201) and the Industrial Strategic technology development program (10041618, Development of Needle Insertion Type Image-based Interventional Robotic System for Biopsy and Treatment of 1 cm Abdominal and Thoracic Lesion with Reduced Radiation Exposure and Improved Accuracy) funded by the Ministry of Trade Industry and Energy, Korea.

References

[1] Lim M A, Kim D H, Park C O, Lee Y W, Han S W, Li Z, Williams R S and Park I 2012 A new route toward ultrasensitive, flexible chemical sensors: metal nanotubes by wet-Chemical synthesis along sacrificial nanowire templates *ACS Nano* **6** 598–608

[2] Curto V F, Fat C, Coyle S, Byrne R, O'Toole C, Barry C, Hughes S, Moyna N, Diamond D and Benito-Lopez F 2012 Real-time sweat pH monitoring based on a wearable chemical barcode micro-fluidic platform incorporating ionic liquids *Sensors Actuators* B **171–172** 1327–34
[3] Tormene P, Bartolo M, De Nunzio A M, Fecchio F, Quaglini S, Tassorelli C and Sandrini G 2012 Estimation of human trunk movements by wearable strain sensors and improvement of sensor's placement on intelligent biomedical clothes *Biomed. Eng. Online* **11** 95
[4] Giorgin T, Lorussi F, Rossi D D and Quaglini S 2006 Posture classification via wearable strain sensors for neurological rehabilitation *Proc. 28th IEEE EMBS Ann. Int. Conf.* (*New York, NY*)
[5] Byun D, Cho S J and Kim S 2013 Fabrication of a flexible penetrating microelectrode array for use on curved surfaces of neural tissues *J. Micromech. Microeng.* **23** 125010
[6] Mishra V, Schned A R, Hartov A, Heaney J A, Seigne J and Halter R J 2013 Electrical property sensing biopsy needle for prostate cancer detection *Prostate* **73** 1603–13
[7] Lee T M, Hur S, Kim J H and Choi H C 2010 EL device pad-printed on a curved surface *J. Micromech. Microeng.* **20** 015016
[8] Moon H C, Lodge T P and Frisbie C D 2014 Solution-processable electrochemiluminescent ion gels for flexible, low-voltage, emissive displays on plastic *J. Am. Chem. Soc.* **136** 3705–12
[9] Kim T H 2011 Full-colour quantum dot displays fabricated by transfer printing *Nat. Photon.* **5** 176–82
[10] Koo M, Park K I, Lee S H, Suh M, Jeon D Y, Choi J W, Kang K and Lee K J 2012 Bendable inorganic thin-film battery for fully flexible electronic systems *Nano Lett.* **12** 4810–6
[11] Gaikwad A M, Whiting G L, Steingart D A and Arias A C 2011 Highly flexible, printed alkaline batteries based on mesh-embedded electrodes *Adv. Mater.* **23** 3251–5
[12] Kim J G, Takama N, Kim B J and Fujita H 2009 Optical-softlithographic technology for patterning on curved surfaces *J. Micromech. Microeng.* **19** 055017
[13] Ahn C H, Park H W, Kim H H, Park S H, Son C, Kim M C, Lee J H and Go J S 2013 Direct fabrication of thin film gold resistance temperature detection sensors on a curved surface using a flexible dry film photoresist and their calibration up to 450 °C *J. Micromech. Microeng.* **23** 065031
[14] Jackman R J, Wilbur J L and Whitesides G M 1995 Fabrication of submicrometer features on curved substrates by microcontact printing *Science* **269** 664–6
[15] Goluch E D, Shaikh K A, Ryu K, Chen J, Engel J and Liu C 2004 Microfluidic method for *in-situ* deposition and precision patterning of thin-film metals on curved surfaces *Appl. Phys. Lett.* **85** 3629–31
[16] Yoon S, Choi K, Baek S and Chang H 2011 Electronic circuit patterning on curved surface by direct laser structuring *Proc. Int. Conf. on Electrical Machines and Systems (ICEMS)* (*Beijing, China*)
[17] Adams J J, Duoss E B, Malkowski T F, Motala M J, Ahn B Y, Nuzzo R G, Bernhard J T and Lewis J A 2011 Conformal printing of electrically small antennas on 3D surfaces *Adv. Mater.* **23** 1335–40
[18] Farahani R D, Chizari K and Therriault D 2014 3D printing of freeform helical microstructures: a review *Nanoscale* **6** 10470
[19] Chen D, Zhao L, Diao H, Zhang W, Wang G and Wang W 2014 Low-temperature sintering properties of the screen-printed silver paste for a-Si:H/c-Si heterojunction solar cells *J. Mater. Sci.: Mater. Electron.* **25** 2657–64
[20] Tan K S and Cheong K Y 2014 Physical and electrical characteristics of silver-copper nanopaste as alternative die-attach *IEEE Trans. Compon. Packaging Manuf. Technol.* **4** 8–15
[21] Jeong S, Song H C, Lee W W, Choi Y, Lee S S and Ryu B H 2010 Combined role of well-dispersed aqueous Ag ink and the molecular adhesive layer in inkjet printing the narrow and highly conductive Ag features on a glass substrate *J. Phys. Chem.* C **114** 22277–83
[22] Yacoub J H, Verma S, Moulton J S, Eggener S and Oto A 2012 Imaging-guided prostate biopsy: conventional and emerging techniques *Radiographics* **32** 819–37
[23] Diamantis A, Magiorkinis E and Koutselini H 2009 Fine-needle aspiration (FNA) biopsy: historical aspects *Folia Histochem. Cytobiol.* **47** 191–7
[24] Laurent F, Montaudon M, Latrabe V and Begueret H 2003 Percutaneous biopsy in lung cancer *Eur. J. Radiol.* **45** 60–8
[25] Halter R J, Schned A, Heaney J, Hartov A and Paulsen K D 2009 Electrical properties of prostatic tissues: I. single frequency admittivity properties *J. Urol.* **182** 1600–7
[26] Halter R J, Schned A, Heaney J, Hartov A and Paulsen K D 2009 Electrical properties of prostatic tissues: II. spectral admittivity properties *J. Urol.* **182** 1608–13
[27] Gabriel C, Gabriel S and Corthout E 1996 The dielectric properties of biological tissues: I. Literature survey *Phys. Med. Biol.* **41** 2231–49
[28] Xu T, Zach M P, Xiao Z L, Rosenmann D, Welp U, Kwok W K and Crabtree G W 2005 Self-assembled monolayer-enhanced hydrogen sensing with ultrathin palladium films *Appl. Phys. Lett.* **86** 203104
[29] Sakamoto Y, Takai K, Takashima I and Imada M 1996 Electrical resistance measurements as a function of composition of palladium–hydrogen(deuterium) systems by a gas phase method *J. Phys.: Condens. Matter* **8** 3399–411